2026 IEEE/SICE International Symposium on System Integration (SII)
January 11-14, 2026. Cancún, México

Development of Miniature Model of Container Crane for Remote Operation and Automation

Rintaro Ozaki[1], Naoyuki Takesue[1], and Fukiko Kawai[2]

***Abstract*— Although container cranes are essential to port logistics, issues remain regarding operational efficiency and safety. These issues are caused by factors such as aging operators, labor shortages, and sway caused by strong winds, acceleration, and deceleration. In particular, in the development and evaluation of remote operation and automation systems for container cranes involves high costs and strict safety restrictions, which reduces development efficiency. Therefore, this study designed and manufactured a small-scale crane model at approximately one-thirtieth the actual size and evaluated its operation. As initial steps toward remote operation and automation, remote control and automation control systems were constructed using the small-scale crane. The feasibility of basic operations was confirmed. Furthermore, the position of the spreader was estimated using LiDAR, and its effectiveness was verified.**

I. Introduction

In international logistics, more than four-fifths of global trade volume is carried by maritime transport [1]. From this, it follows that ports play a pivotal role as core hubs connecting maritime and land transportation. Among them, container transportation has made cargo handling more efficient by using standardized containers. One of the core pieces of equipment is the container crane, which is indispensable for quickly and safely transferring a large number of containers from ship to shore or from shore to ship.

In recent years, cranes have generally faced challenges such as the aging operator population, labor shortages, and harsh working environments. Container cranes are no exception, and port work is easily affected by external factors such as waves and strong winds because ports are located near the sea. Since the spreader that grips containers is suspended by wires, it sways easily under external disturbances or during the acceleration and deceleration of the trolley. Such sway reduces both the efficiency and safety of cargo handling, and requires highly experienced and skilled operators. However, acquiring these skills requires long-term training, which further worsens the problem of labor shortages.

Against this background, there is an increasing demand for remote operation and automation of cargo handling, and related studies have been conducted[2], [3], [4], [5], [6], [7]. However, in the development and performance evaluation of container crane systems, the use of actual cranes entails high costs and significant safety constraints, leading to reduced development efficiency. Therefore, the use of simulation and small-scale crane models that enable evaluation without relying on actual cranes is considered an effective approach[8], [9].

Fig. 1: Appearance of the container crane

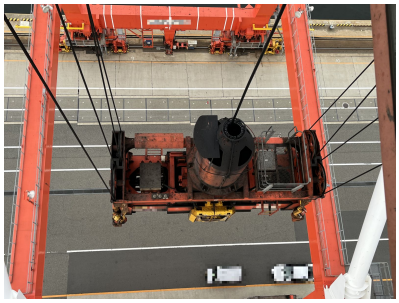

Fig. 2: Top view of the spreader

In this study, a small-scale crane model at approximately $1/30$ of the actual size was designed and manufactured, and its operation was evaluated. Furthermore, as an initial step toward remote operation and automation, a remote-control system and an automation-control system were constructed using this small-scale model. In addition, the sway of the spreader was measured using LiDAR, aiming for future applications such as automatic obstacle detection and spreader localization.

II. Crane Configuration

A. Overview

The container crane considered in this study is shown in Fig. 1. The top view of the spreader that grips the container is shown in Fig. 2.

In this study, to realize remote operation and automation of cargo handling using container cranes, a small-scale crane

[1]Rintaro Ozaki and Naoyuki Takesue are with Tokyo Metropolitan University, Hino-shi, Tokyo, Japan. [2]Fukiko Kawai is with Fuji Electric Co., Ltd.

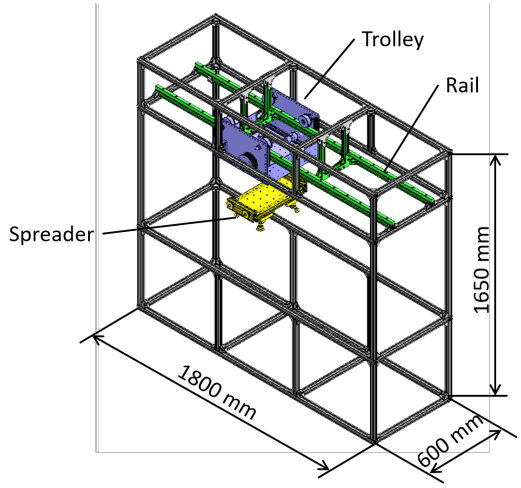

Fig. 3: CAD drawing of the small-scale crane

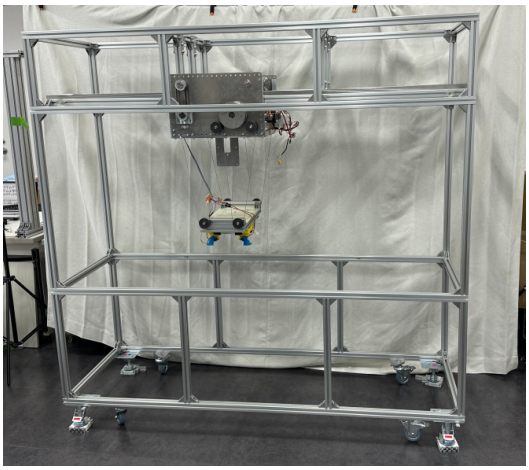

Fig. 4: Appearance of the small-scale crane

model at approximately $1/30$ of the actual size was designed and manufactured. Since evaluating the system with an actual crane would be difficult and hazardous in terms of both safety and cost, the design was carried out using a small-scale model. This small-scale model can simulate the operation of the actual crane, enabling easy development and verification of remote operation systems, automation systems, and control algorithms. Fig. 3 shows the CAD drawing of the small-scale crane, and Fig. 4 shows its appearance.

The small-scale crane system is designed to support training for remote operation and to evaluate the effectiveness of automation systems. It is equipped with traversing, hoisting, and gripping functions. The system consists of a trolley that moves horizontally along rails, a spreader suspended from the trolley by wire ropes to grip containers, and the rails on which the trolley travels. By controlling the trolley, both the horizontal motion and the vertical motion of the spreader can be achieved, enabling the reproducibility of cargo-handling operations at a small-scale. However, because the wire length of the spreader in the small-scale crane is shorter than that of a actual crane, resulting in shorter sway period and faster

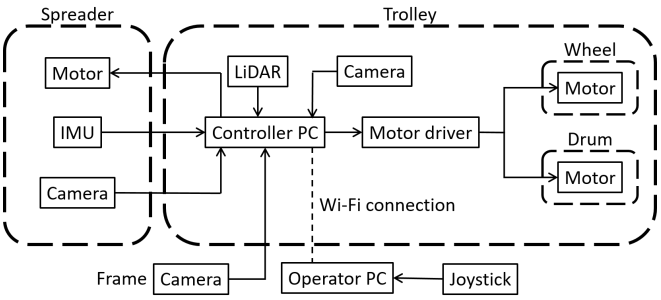

Fig. 5: System configuration

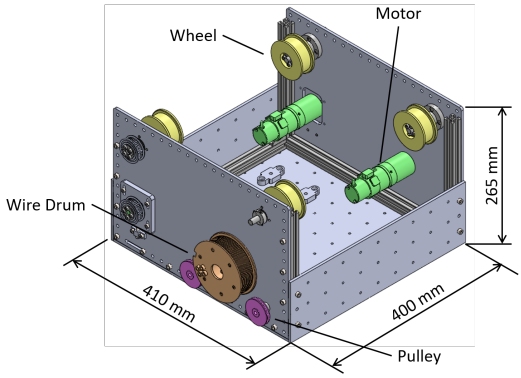

Fig. 6: Appearance of the trolley

spreader oscillations.

Fig. 5 shows the system configuration. Motor control is performed by the controller PC mounted on the trolley. In manual operation, joystick input from the operator PC is transmitted to the controller PC via Wi-Fi, and motor control is executed based on those commands. In automatic operation, information obtained from sensors such as LiDAR and cameras is used to detect container positions, obstacles, and the sway of the spreader, and motor control is executed based on the detection results.

Next, the trolley and spreader, which are the main components of the small-scale crane, are described.

B. Trolley

The appearance of the trolley is shown in Fig. 6.

The trolley is equipped with four wheels, two on each side, to travel along two rails, allowing horizontal movement along the rails. One is the drive wheel, and the other is the passive wheel. In addition, the trolley is equipped with two winding drums, one on each side, which raise and lower the wire suspending the spreader. This enables the vertical motion of the spreader.

For driving the wheels and drums, servo motors (model RH-11D-6001-E100AL) manufactured by Harmonic Drive Systems, Inc. are used. The rated rotation speed of the motor is $60\,\mathrm{rpm}$, the wheel diameter is $60\,\mathrm{mm}$, and the drum diameter is $100\,\mathrm{mm}$. Therefore, the rated traversing speed of the trolley is approximately $0.188\,\mathrm{m/s}$, and the rated hoisting speed of the spreader is approximately $0.314\,\mathrm{m/s}$.

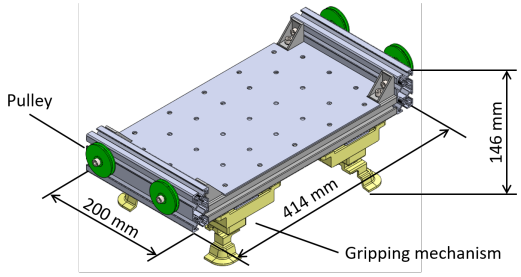

Fig. 7: Appearance of the spreader

The motor control adopts velocity control implemented by I-P control as the following.

$$\tau = K_i \int (\omega_d - \omega)dt - K_p\omega \tag{1}$$

Where τ is the motor torque, ω_d is the reference angular velocity of the motor, ω is the output angular velocity of the motor, K_p the proportional gain, and K_i the integral gain.

Furthermore, for trolley position control, the position error was multiplied by a proportional gain to form the motor's reference angular velocity, thereby constituting an overall PID control system.

$$\omega_d = K_P(x_d - x) \tag{2}$$

Where K_P is the position proportional gain. Furthermore, x_d is the trolley's reference position, and due to the wheel diameter D_w and the motor reference angle θ_d, the relationship $x_d = D_w\theta_d$ holds. Similarly, x is the trolley's current position, and it has the relationship $x = D_w\theta$ with the motor's current angle θ.

C. Spreader

The appearance of the spreader is shown in Fig. 7.

The spreader is equipped with four pulleys, two on each side, through which the wires are passed. These wires are connected to the drums mounted on the trolley, and by rotating the drums, the spreader can be raised and lowered.

Furthermore, container gripping mechanisms are installed at the four corners of the bottom of the spreade. By rotating the output shaft of the servo motor by $90°$, the claw attached to the shaft engages with the corner casting on the top of the container, thereby enabling the container to be gripped.

Similar to the trolley, the spreader's velocity and position controls also employed PID control.

III. Evaluation of the Small-Scale Crane

To verify that the basic motions of the small-scale crane operated as intended, such as traversing and hoisting, each function was evaluated individually. Evaluation experiments were conducted on the trolley's speed and position control and the spreader's height control. In addition, the sway of the spreader was examined.

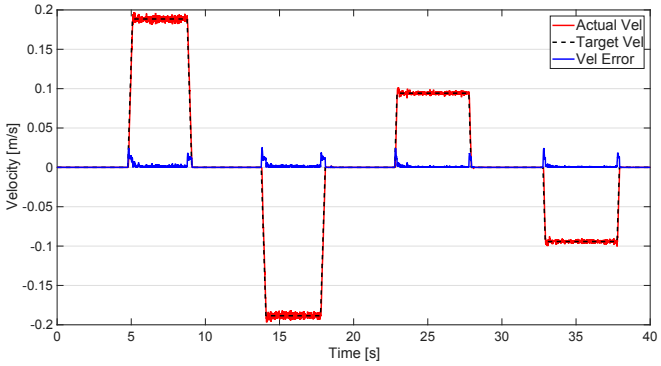

Fig. 8: Comparison between the reference velocity and output velocity of the trolley

A. Velocity Control of the Trolley

A reference velocity was input to the trolley, and it was evaluated whether the actual velocity converges to the reference velocity. The acceleration of the trolley was set to $0.3\,\mathrm{m/s^2}$, and the output velocity was calculated from the encoder. The comparison between the reference velocity and the output velocity is shown in Fig. 8. The difference between the input and the output velocities is also shown.

From Fig. 8, it can be confirmed that the output velocity of the trolley appropriately follows the reference velocity. These results demonstrate that the velocity control system using I-P control provides stable response characteristics in trolley traversing.

B. Position Control of the Trolley

To evaluate the position control performance of the trolley, a target position was provided, and it was verified whether the actual position converged to the target value. The initial position of the trolley was set to $0\,\mathrm{m}$, and the acceleration was set to $0.3\,\mathrm{m/s^2}$. The output position was measured using a motion capture system. In addition, the position calculated from the encoder was also obtained. The comparison between the reference position and these output positions is shown in Fig. 9. The difference between the position obtained by motion capture and that calculated from the encoder is also shown.

Fig. 9 confirms convergence to the reference position and shows that the trolley has good tracking performance in position control. However, the difference between the position obtained by motion capture and that calculated from the encoder was $0.013\,\mathrm{m}$. Since the small-scale crane is approximately $1/30$ of the actual machine, this corresponds to about $0.39\,\mathrm{m}$ in the actual crane. Such an error may affect accurate positioning of the spreader and obstacle avoidance during cargo-handling operations.

The cause of this error is considered to be slippage between the wheels and rails. When operated manually, the trolley is controlled to visually correct the spreader's position. Since slippage can always occur due to surface conditions or acceleration and deceleration, future control design must incorporate compensation for its effects.

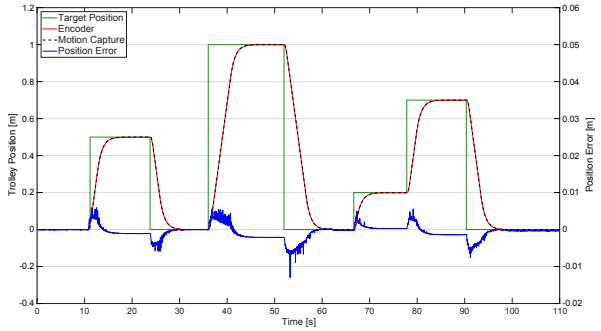

Fig. 9: Position of trolley

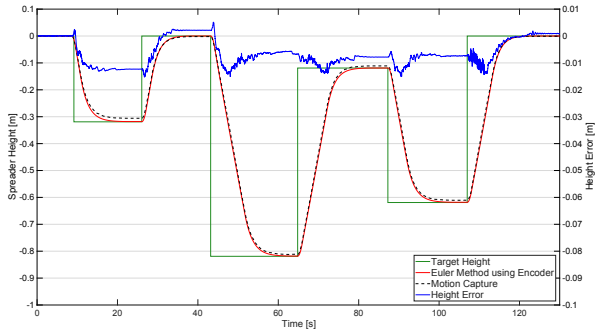

Fig. 10: Height of spreader

C. Height Control of the Spreader

To evaluate the height control performance of the spreader, a target position was provided, and it was verified whether the actual height converged to the target value. The initial height of the spreader was set to $0\,\mathrm{m}$, and the acceleration was set to $0.3\,\mathrm{m/s^2}$. The output height was measured using a motion capture system. In addition, since the wire feed amount calculated from the encoder does not have a simple proportional relationship with the spreader height, the spreader height was numerically obtained using Euler ' s method based on the wire feed amount. The comparison between the reference height and these output heights is shown in Fig. 10. The difference between the height obtained by motion capture and that obtained by Euler's method is also shown.

Although the spreader approached the reference height, the result indicates that some error remained. Furthermore, the maximum difference between the height obtained by motion capture and that obtained by Euler ' s method was $0.015\,\mathrm{m}$. These errors are considered to be caused by numerical error inherent in Euler ' s method. In addition, while the initial orientation of the spreader was horizontal, it is considered that the spreader tilted during hoisting, resulting in a change in its orientation. These results highlight the need for a system that periodically readjusts the spreader height at fixed intervals to prevent errors from accumulating.

D. Sway of the Spreader

An experiment was conducted to evaluate the displacement of the spreader relative to the trolley, caused by the acceleration and deceleration of the trolley. The vertical distance from the pulley on the trolley side to the pulley on the spreader side is denoted as l_{ts}. A measurement was taken under the condition of $l_{ts} = 0.5\,\mathrm{m}$. The trolley was moved forward $1.0\,\mathrm{m}$ from its initial position and then returned to the initial position. PID control was used for position control, and the maximum acceleration of the trolley was set to $0.3\,\mathrm{m/s^2}$. The positions of the trolley and spreader were measured using motion capture, and for analysis, only the displacement component of the spreader relative to the trolley along the travel direction was extracted. The displacement results of the spreader are shown in Fig. 11. The input velocity of the trolley is also indicated.

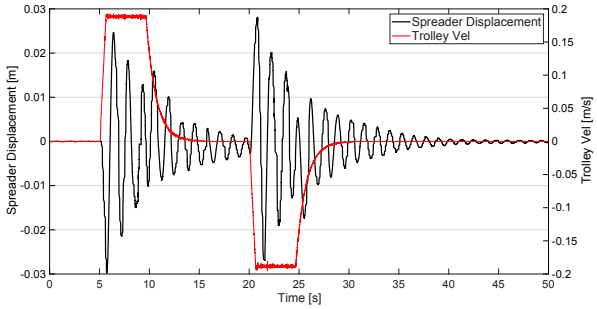

Fig. 11: Displacement results of the spreader relative to the trolley

From Fig. 11, it can be confirmed that the sway of the spreader increased significantly immediately after the start of trolley acceleration and deceleration. The maximum displacement was $0.038,\mathrm{m}$ for $l_{ts} = 0.5,\mathrm{m}$. Converted to the actual crane, this corresponds to approximately $1.14,\mathrm{m}$. These results indicate that the sway of the spreader causes substantial difficulty in gripping containers, and therefore represents a critical issue in control system design.

Note that for the purpose of functional verification in this experiment, simple PID control was used; however, sway suppression control will be introduced in the future.

IV. Remote Operation and Automaric Control of the Crane

The small-scale crane is equipped with cameras mounted on the crane frame, the lower part of the trolley, and the front of the spreader. These cameras allow the operator to simultaneously view images from each perspective on the operator PC. Fig. 12 shows the operator PC displaying the camera images. By capturing images from multiple viewpoints, the operator can grasp the relative position between the container and the spreader, as well as detect obstacles around the spreader or container, enabling a clear understanding of the site conditions. Furthermore, by using a joystick connected to the operator PC, the operator can remotely control each motion of the crane. In this way, the operator can monitor and control the crane from a remote location, eliminating the need to be physically onboard the container crane and enabling safe cargo handling operations through remote control.

By limiting the camera to only the lower part of the trolley,

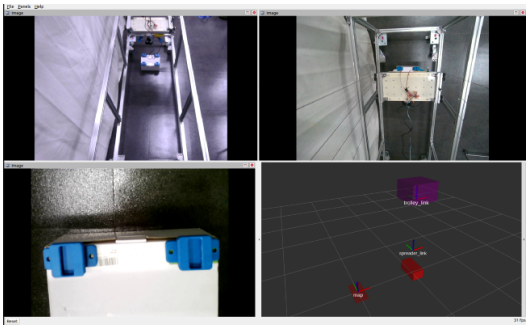

Fig. 12: Operator PC display

it is possible to reproduce the same viewpoint as during onboard operation of the actual crane. Thus, the small-scale crane can also be used for training purposes in cargo handling operations. Because training can be conducted without using the actual crane, it not only ensures safety but also provides effective and efficient educational outcomes. Note that the wire length differs from that of an actual crane, so the pendulum's oscillation period is different.

Furthermore, as an initial step toward full automation, automatic movement of the container was performed according to pre-set container positions and heights. An example of the automatic cargo handling operation is shown in Fig. 13. Fig. 13(a) shows the spreader in its initial position at the top left. Fig. 13(b) shows the spreader lowered onto the container on the right. Fig. 13(c) shows the spreader reaching the container. Fig. 13(d) shows the spreader lifting the container. Fig. 13(e) shows the spreader moving the container to the left. Fig. 13(f) shows the spreader lowering the container at the target position on the left. Fig. 13(g) shows the container being landed, Fig. 13(h) shows the container being released and the spreader being raised.

Through this sequence, it was confirmed that automatic control can successfully transport containers based on the specified positions and heights.

V. Measurement of Spreader Oscillation Using LiDAR

As shown in Fig. 11, the spreader oscillates due to the acceleration and deceleration of the trolley. To suppress this oscillation, it is necessary to measure the motion of the spreader. In this study, an RS-LiDAR-16 (RoboSense) was mounted under the trolley. By installing the LiDAR on the trolley, containers located not only on land but also on container ship can be detected as the trolley moves. Moreover, placing the sensor at a high position reduces blind spots and is expected to improve the detection of objects and obstacles. In this experiment, this LiDAR is used to measure the sway of the spreader. The overview of the measurement method is as follows:

- Filter the point cloud obtained from the LiDAR and extract the points corresponding to the top surface of the spreader.
- Project the extracted points onto the XY plane and divide them into blocks along the trolley travel direction.

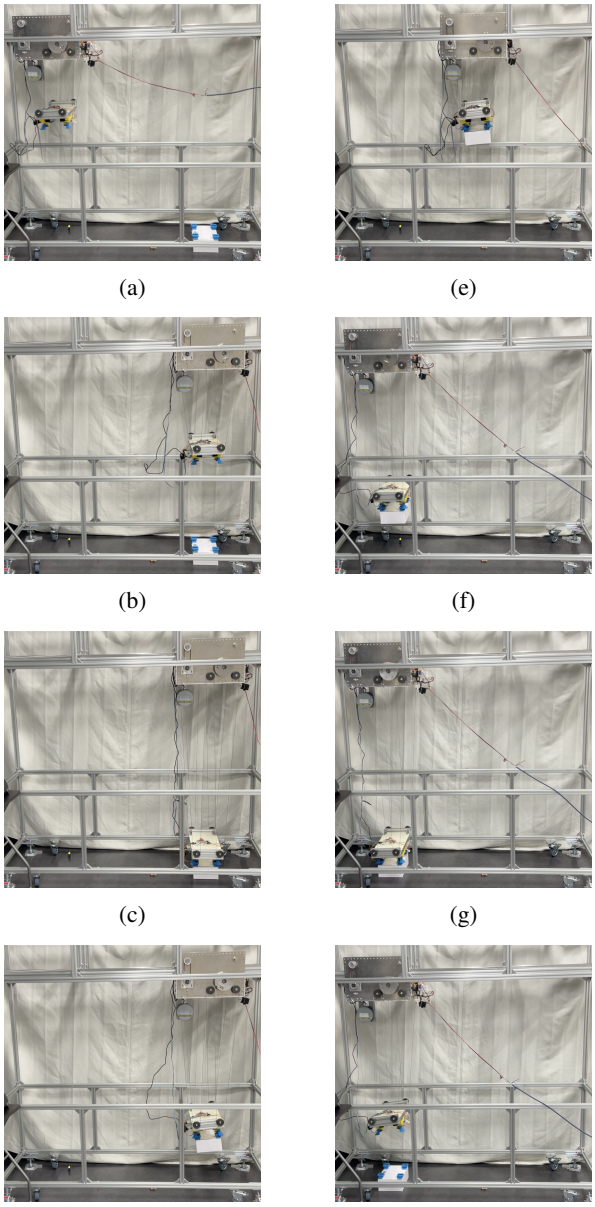

Fig. 13: Sequence motion of automatic operation

- For each block, extract the points at both ends of the spreader along the travel direction (maximum and minimum points) as candidate edge points.
- Perform line fitting based on RANSAC for the two sequences of edge candidate points, remove outliers, and obtain more accurate edge points.
- Calculate the centroid of the spreader top surface from the edge point cloud.

To verify the effectiveness of this method, an evaluation experiment was conducted. From the perspective of oscillation frequency, it should be noted that the small-scale crane operates under more stringent conditions than an actual crane. In the experiment, the spreader was manually oscillated, and the oscillation was measured simultaneously

using this method and a motion capture system. The vertical distance l_{ts} from the trolley pulley to the spreader pulley was fixed at $1.0\,\mathrm{m}$. The comparison results are shown in Fig. 14. The data acquisition rate of the motion capture system was $120\,\mathrm{Hz}$, while that of the LiDAR was $10\,\mathrm{Hz}$, resulting in a difference in the number of data points. Therefore, the motion capture data was linearly interpolated to match the LiDAR acquisition times. This aligned the time axes, and the difference between them was calculated.

Fig. 14 shows that the measurements obtained by this method and the motion capture system generally agree well. However, a maximum difference of $0.076\,\mathrm{m}$ was observed. Three main factors are considered to contribute to this difference:

First, the sensor measurement accuracy. The position accuracy of the LiDAR accuracy is around $20\,\mathrm{mm}$. Thus, measurement error from the LiDAR likely contributes to the observed difference.

Second, approximation error due to linear interpolation. Since the acquisition rates of the two systems differ, the motion capture data were linearly interpolated to match the LiDAR timing for comparison. However, interpolation approximates inherently nonlinear oscillatory motion with straight lines, which may introduce errors, especially during large amplitude oscillations or acceleration/deceleration.

Third, the limited number of points in the point cloud. The method extracts edge points from the top surface of the spreader to calculate the centroid. Due to the small number of points obtained from the LiDAR, biased point distributions may introduce systematic errors in the centroid calculation.

Therefore, the observed differences between this method and the motion capture system are considered to result from sensor accuracy limits, interpolation-induced approximation errors, and calculation errors due to insufficient point cloud data.

In future work, combining an IMU is considered to estimate oscillations that cannot be fully captured by LiDAR alone, improving measurement accuracy. In particular, small displacements occurring between LiDAR sampling intervals could be complemented using high-frequency IMU data. Furthermore, projecting the spreader point cloud onto a plane parallel to the spreader top, rather than the XY plane, would allow shape-consistent point cloud processing and reduce outliers among the edge candidate points. This approach is expected to extract a larger number of reliable points and improve centroid calculation accuracy.

VI. Conclusion

In this study, a small-scale crane model at approximately 1/30 of the actual crane was designed and fabricated, and its fundamental operations were evaluated. Although the vibration periods differ due to the varying wire lengths between actual and small-scale cranes, the following phenomena that could occur in actual equipment were confirmed. The results confirmed that wheel slippage occurs in the trolley position control and numerical errors arise in spreader height control, indicating the need for future compensation. It was also

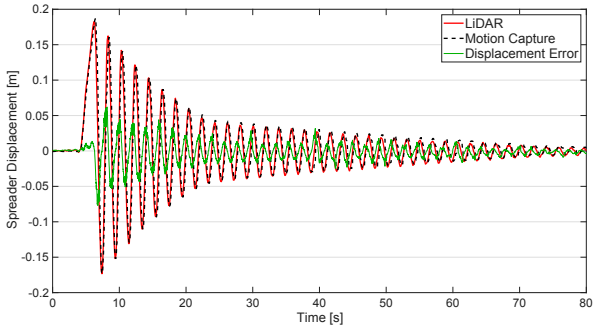

Fig. 14: Comparison of spreader oscillation measurements

confirmed that oscillatory behavior during acceleration and deceleration in cargo handling operations can be reproduced. Furthermore, initial remote operation and automatic control systems were established, demonstrating basic functionality. As an experiment toward automation, spreader oscillation measurement using LiDAR was conducted, confirming that oscillatory behavior can be successfully measured.

These results suggest that the small-scale crane is an effective and safe tool for low-cost performance evaluation in the development of remote operation and automation systems for container cranes. Future work will focus on developing advanced automatic control algorithms that use LiDAR, cameras, and an IMU. These algorithms will be evaluated in wind disturbance conditions that more closely resemble real environments. The goal is to automate container cranes.

References

[1] United Nations Conference on Trade and Development. Review of maritime transport 2023. Technical report, United Nations Conference on Trade and Development (UNCTAD), 2023.

[2] Nenad Zrnić, Zoran Petković, and Srđan Bošnjak. Automation of ship-to-shore container cranes: A review of stateof-the-art. *FME Transactions*, 33:111–121, 2005.

[3] Hiroshi ITO and Kohei SUZUKI. Sway control of overhead travelling crane considering coupled vibration. *Transactions of the Japan Society of Mechanical Engineers Series C*, 72(720):2406–2412, 2006. (in Japanses).

[4] Takanori Miyoshi, Yoshiyuki Noda, and Kazuhiko Terashima. Feedforward control considering input and states constraints with eliminating residual vibration. In *2007 American Control Conference*, pages 5005–5010, 2007.

[5] H. Kawai, Y. Choi, Y. B. Kim, and Y. Kubota. Position measurement of container crane spreader using an image sensor system for anti-sway controllers. In *2008 International Conference on Control, Automation and Systems*, pages 683–686, 2008.

[6] Noriaki MIYATA. Up Grade of Remote Automated RTG (Pursuit of faster, more accurate and safer automated container handling). Technical report, Sumitomo Heavy Industries Technical Review, 2020. (in Japanses).

[7] A. Arena, A. Casalotti, W. Lacarbonara, and M. P. Cartmell. Dynamics of container cranes: three-dimensional modeling, full-scale experiments, and identification. *International Journal of Mechanical Sciences*, 93:8–21, 2015.

[8] A. Arena, A. Casalotti, W. Lacarbonara, and M.P. Cartmell. Dynamics of container cranes: three-dimensional modeling, full-scale experiments, and identification. *International Journal of Mechanical Sciences*, 93:8–21, 2015.

[9] Rini Nur Hasanah, M. Firsada Putra Perdana, Rari Santoso, and Hadi Suyono. Design and construction of a single-arm crane miniature for stevedoring. In *2017 20th International Conference on Electrical Machines and Systems (ICEMS)*, pages 1–6, 2017.